Astronomy & Astrophysics manuscript no. numax_v4.6.1
December 13, 2019

Unveiling the power spectrum of δ Scuti stars with *TESS*

The temperature, gravity, and frequency scaling relation

S. Barceló Forteza[1], A. Moya[2,3], D. Barrado[1], E. Solano[1,4], S. Martín-Ruiz[5], J. C. Suárez[6,5], and A. García Hernández[6,5]

[1] Dpto. de Astrofísica, Centro de Astrobiología (CSIC-INTA), ESAC, Camino Bajo del Castillo s/n, 28692, Spain
[2] Electrical Engineering, Electronics, Automation and Applied Physics Department, E.T.S.I.D.I, Polytechnic University of Madrid (UPM), Madrid 28012, Spain
[3] School of Physics and Astronomy, University of Birmingham, B15 2TT, UK.
[4] Spanish Virtual Observatory, Spain
[5] Instituto de Astrofísica de Andalucía (CSIC), Glorieta de la Astronomía s/n, 18008, Granada, Spain
[6] Dept. Theoretical Physics and Cosmology, University of Granada (UGR), 18071, Granada, Spain

Received 5 December 2019; Accepted

ABSTRACT

Thanks to high-precision photometric data legacy from space telescopes like *CoRoT* and *Kepler*, the scientific community could detect and characterize the power spectra of hundreds of thousands of stars. Using the scaling relations, it is possible to estimate masses and radii for solar-type pulsators. However, these stars are not the only kind of stellar objects that follow these rules: δ Scuti stars seem to be characterized with seismic indexes such as the large separation ($\Delta\nu$). Thanks to long-duration high-cadence *TESS* light curves, we analysed more than two thousand of this kind of classical pulsators. In that way, we propose the frequency at maximum power ($\nu_{\rm max}$) as a proper seismic index since it is directly related with the intrinsic temperature, mass and radius of the star. This parameter seems not to be affected by rotation, inclination, extinction or resonances, with the exception of the evolution of the stellar parameters. Furthermore, we can constrain rotation and inclination using the departure of temperature produced by the gravity-darkening effect. This is especially feasible for fast rotators as most of δ Scuti seem to be.

Key words. asteroseismology - stars: oscillations - stars: variables: δ Scuti

1. Introduction

Asteroseismology has proven to be a very fruitful technique to characterize the stars. The seismic indexes describe the properties of the power-spectral structure as a whole, the so-called power spectrum envelope (envelope hereafter). The scaling relations can relate their structural parameters with seismic indexes such as happens with solar-like pulsators (e.g., Kjeldsen & Bedding 1995). Using the high amount of stellar data from space missions like *CoRoT* (Baglin et al. 2006) or *Kepler* (Borucki et al. 2010), the scientific community has been looking for scaling relations also for δ Scuti stars (e.g., Suárez et al. 2014; García Hernández et al. 2015; Michel et al. 2017; Moya et al. 2017; Barceló Forteza et al. 2018; Bowman & Kurtz 2018). Trying to extend ensemble asteroseismology, Barceló Forteza et al. (2018, -BF18 hereafter-) describe the envelope of δ Scuti stars with several magnitudes such as the number of modes ($N_{\rm env}$), the frequency at maximum power,

$$\nu_{\rm max} = \frac{\sum A_i \nu_i}{\sum A_i}\,, \tag{1}$$

where ν_i and A_i are the frequency and the amplitude of each mode of the envelope, respectively; and its asymmetry

$$\alpha = \frac{2\nu_{\rm max} - \nu_h - \nu_l}{2\,(\nu_h - \nu_l)}\,, \tag{2}$$

where $\nu_{h/l}$ are the highest and lowest frequency of the envelope, respectively.

δ Scuti stars are A-F intermediate mass stars (1.5 to 2.5 $M_\odot$; Breger 2000a) with frequencies between 60 to 930 μHz and temperatures from 6000 to 9000 K (Uytterhoeven et al. 2011). Their main excitation mechanism is κ-mechanism (Chevalier 1971). Dziembowski (1997) predicted that the excited modes have higher frequencies at higher temperatures ($T_{\rm eff} \propto \nu_i$, see Fig. 2 in that paper). Taking into account solar composition, but no rotation, and no core overshoot, Balona & Dziembowski (2011) also predicted this behaviour for the frequency of the mode with highest amplitude,

$$T_{\rm eff} \propto \nu_0\,. \tag{3}$$

However, the observations show a wide variation (see Fig. 2 in that paper). These differences may be produced by other mechanisms playing a significant role, especially for hybrid pulsators (Antoci et al. 2014; Xiong et al. 2016). On the other hand, there are other physical processes that can modify the temperature we observe such as the gravity-darkening effect (von Zeipel 1924). A high rotation rate can modify the shape of the star from a sphere to an ellipsoid. In that way, the temperature at the poles will be higher than the temperature at the equator. The departure of temperature is defined by BF18 as

$$\delta\bar{T}_{\rm eff}(i) \equiv \frac{T_{\rm eff}(i) - \bar{T}_{\rm eff}}{\bar{T}_{\rm eff}} \approx \left(\frac{1 - \frac{R(i)}{R}\epsilon^2 \sin^2\{i\}}{1 - \frac{2}{3}\epsilon^2}\right)^{\frac{\beta}{4}} - 1 \tag{4}$$

where i is the inclination from the line of sight; β depends on the importance of the convection (Claret 1998); and ϵ is the ratio

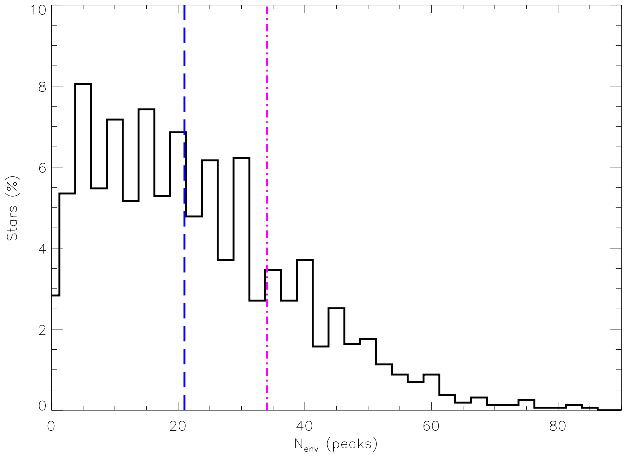

Fig. 1. Distribution of stars according to the number of peaks in their envelope. Dashed blue line points to the mean number of peaks of the envelope and the purple dashed-dotted to the estimated by Lignières & Georgeot (2009).

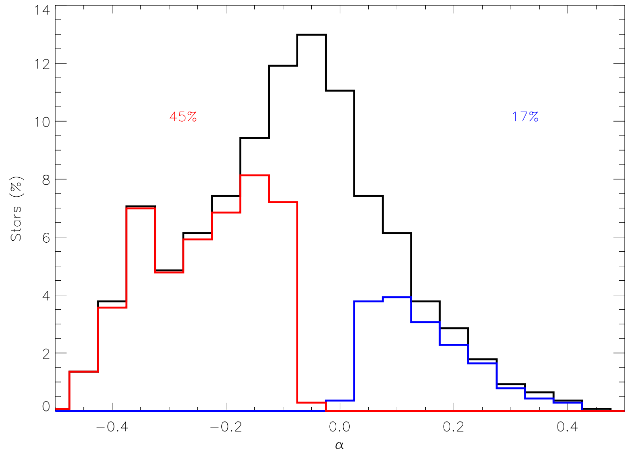

Fig. 2. Distribution of stars according to their asymmetry (black histogram). Blue (Red) histogram denotes the proportion of stars whose $\nu_{\rm max}$ deviation from the mean frequency of the envelope towards lower (higher) frequencies is significantly higher than the solar case (see text).

between the centrifugal and gravity forces

$$\epsilon^2 = \frac{\Omega^2 R^3}{GM} \tag{5}$$

where M is the mass; $\bar{T}_{\rm eff}$ and R are the mean effective temperature and the mean radius, i.e., the temperature and radius of a spherically symmetric star with the same mass than the rotating star. The value of the departure of temperature is positive (negative) for inclinations lower (higher) than mid-latitudes ($i \sim 55°$) and higher its value with higher rotation rate up to the break-up frequency ($\Omega \sim \Omega_C$). Then, the departure can be up to $\delta\bar{T}_{\rm eff}(i \sim 0°) \sim 14.5\%$ for pole-on and down to $\delta\bar{T}_{\rm eff}(i \sim 90°) \sim -21.5\%$ for edge-on pure δ Scuti stars. At mid-latitudes the non-spherical contributions of all structural parameters are the same as a spherically symmetric star (Pérez Hernández et al. 1999). Balona & Dziembowski (2011) studied the excitation mechanism without taking into account Ω and i. Therefore, we assume that equation 3 may be rewritten as

$$\bar{T}_{\rm eff} \propto \nu_0 \,. \tag{6}$$

Moreover, the mode with highest amplitude can change with time due to any amplitude modulation mechanism (e.g., Barceló Forteza et al. 2015; Bowman et al. 2016, see also Section 4.2). Taking into account pure δ Scuti stars only, BF18 use $\nu_{\rm max}$ instead of ν_0 as a seismic index,

$$\bar{T}_{\rm eff} \propto \nu_{\rm max} \,, \tag{7}$$

finding a higher correlation for this scaling relation (see Section 4) and suggesting that gravity-darkening effect may be the cause of the observed dispersion.
Christensen-Dalsgaard (2000) predicted that the age also modify the excited frequencies due to the increase of the stellar radius. Taking into account hybrid δ Scuti stars and no gravity-darkening effect, Bowman & Kurtz (2018) suggested that the $T_{\rm eff}$ - ν_0 scaling relation should be differentiated for different evolutionary stages.

Here we show how both, gravity-darkening effect and the evolutionary stage, may be the causes of the observed dispersion and how we can use the $\nu_{\rm max}$ as a seismic index. In Section 2, we explain which data is used and how is analysed. We present our results for the $\bar{T}_{\rm eff} - \nu_{\rm max}$ scaling relation in Section 3, including how it changes taking into account different values of surface gravity. In Section 4, we discuss why the evolutionary stage may modify the scaling relation and also the gravity-darkening effect. In Section 5, we show the advantages of using the scaling relation to obtain $\bar{T}_{\rm eff}$. Finally, we present our conclusions in Section 6.

2. Data and analysis

Our statistical study needs of a large sample of δ Scuti type stars. For that reason, we analysed a total of 2372 A and F stars with peaks within the typical frequency regime of this type of stars, including those of studied in BF18. We obtained the data from CoRoT Sismo-channel: 8 stars (Charpinet et al. 2006); Kepler Long and Short Cadence light curves: 1124 and 572 stars, respectively (Brown et al. 2011); and TESS satellite from sectors 1 to 11 (668 stars; Stassun et al. 2019). Each sector lasts around ~27 days and the number of sectors depend on the position of the star in the sky. Therefore, the maximum duration of the light curve is of ~300 days. The cadence of the studied TESS light curves is ~2 minutes and, therefore, the Nyquist frequency is 4167 μHz far enough from the typical frequency regime for δ Scuti stars (Aerts et al. 2010).
Using δ Scuti Basics Finder pipeline (δSBF hereafter, Barceló Forteza et al. 2017, and references therein), we characterized their power-spectral structure. Thanks to this method (Barceló Forteza et al. 2015), we interpolate the light curve of each star using the information of the subtracted peaks minimizing the effect of gaps and considerably improving the background noise, thereby avoiding spurious effects (García et al. 2014). Finally, this pipeline produces more accurate and precise results in terms of the parameters of the modes. Its reasonably fast computing speed makes this pipeline appropriate for the study of large samples. We also include a superNyquist analysis (Murphy et al. 2013) up to 1132 μHz only to those light curves with lower Nyquist frequency. We used the same threshold than in BF18 to study the peaks of the envelope, avoiding hundreds of low amplitude peaks that may be part of the grass (e.g., Poretti et al.

Table 1. Parameters of the $\bar{T}_{\rm eff} - \nu_{\rm max}$ relation for each method.

Method[a]	Slope (K/μHz)	Y-intercept (K)	σ (%)	r	P_u (%)	N^b_{in} (%)	N^b_{out} (%)
LFIT[1]	2.94 ± 0.24	6980 ± 50	5.82	0.424	7×10^{-30}	99.3	0.7
LFIT[2]	2.50 ± 0.10	7050 ± 30	5.62	0.551	6×10^{-116}	99.4	0.6
MFIT	3.34 ± 0.17	6890 ± 40	0.81	0.972	13×10^{-19}	99.4	0.6
KFIT	2.50 ± 0.55	7090 ± 120	1.59	0.882	4×10^{-3}	99.4	0.6

Notes. [(a)] See Section 3.1. [(b)] Number of stars in and out of the expected departure of temperature limits taking into account $\Omega \sim \Omega_C$ (see text). [(1)] Values taken from Barceló Forteza et al. (2018). [(2)] Using the current sample.

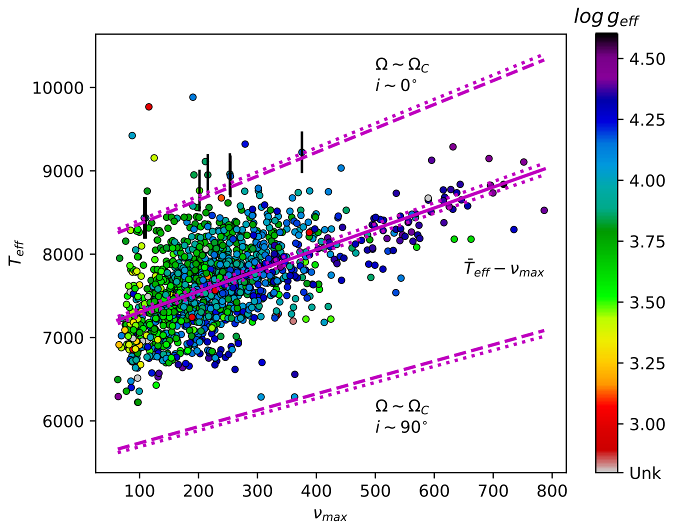

Fig. 3. Relation between $\nu_{\rm max}$ and $\bar{T}_{\rm eff}$ for δ Scuti stars (solid line) using LFIT (see text). The color of each star indicates its measured $g_{\rm eff}$ (Unk is for unknown value). Dashed lines mark the limits of the predicted dispersion due to the gravity-darkening effect. All dashed lines represent the estimated error of the linear fit. We show only the error bars for stars in the limit for clarity.

2009; Barceló Forteza et al. 2017; de Franciscis et al. 2019).

3. Results

After the analysis, we classified the studied stars in δ Scuti, γ Doradus, and hybrid stars, as explained in Uytterhoeven et al. (2011). We find that 1442 of the 2372 stars (∼61%) are δ Scuti stars, 410 stars (∼17%) are δ Sct/γ Dor hybrids, 239 stars (∼10%) are γ Dor/δ Sct hybrids, and 281 stars (∼12%) are γ Doradus stars or other kinds of pulsators. We take into account those stars without significant pulsation in the γ Doradus regime since hybrid stars can have a higher convective efficiency (Uytterhoeven et al. 2011). This is of importance to accomplish all of our assumptions, and only take into account the excitation mechanism of pure δ Scuti stars oscillations.

Regarding the typical number of peaks in the envelopes, we find between 5 to 37 modes and a mean value of 21 modes (see Fig. 1). Using the acoustic ray dynamics, Lignières & Georgeot (2009) estimate the number of island modes and chaotic modes of the power spectra of δ Scuti stars versus the rotation rate. Although its result its only qualitative, we noted that the estimated number of 2-period island modes for a fast-rotating δ Scuti star is of the same order of magnitude (34 ± 2 modes). The observed asymmetry of the envelopes (see Fig. 2) is in agreement with BF18 results. Around 62% of the envelopes have significantly higher asymmetry than the Sun (> 3σ), ∼45% towards lower frequency modes and ∼17% towards higher frequency modes. The higher number of cases towards lower frequencies may be indicative of the excitation mechanism for this kind of stars.

3.1. The $\bar{T}_{\rm eff} - \nu_{\rm max}$ scaling relation

In order to calculate the parameters of this scaling relation we used several techniques. Following the steps in BF18 but including all the stars of the current sample, we made a linear fit between the measured temperatures $T_{\rm eff}$ and $\nu_{\rm max}$ (LFIT, see Table 1 and Fig. 3). To test the probability that the relation between these two parameters is not random, we used the Pearson correlation (r) and the probability of being uncorrelated (P_u; i.e. Taylor 1997). This last parameter represents the probability that N measurements of a priori two uncorrelated variables gives a specific Pearson correlation or higher ($|r| \geq r_0$). For example, in the present case, the probability of being uncorrelated with a Pearson correlation coefficient of $R \sim 0.55$ is around

$$P_u = \frac{2\Gamma\left(\frac{N-1}{2}\right)}{\sqrt{\pi}\Gamma\left(\frac{N-2}{2}\right)} \int_r^1 \left(1 - x^2\right)^{\frac{N-4}{2}} dx \approx 6 \times 10^{-116}\% , \qquad (8)$$

where $\Gamma(x)$ is the gamma function, and N is the number of δ Scuti stars of the sample. Therefore, we find a statistically significant correlation ($P_u \leq 1\%$). In addition, comparing our results from those of BF18, we noted that the higher number of stars of this kind we add, the lower is the probability than these two parameters are uncorrelated although they have similar dispersion values (σ; see Table 1). As BF18 suggest in their study, this dispersion may be produced by gravity-darkening effect since 99.3% of the sample lie inside the expected temperature regime.

For the second technique (MFIT), we calculate the mean effective temperature for each 10 μHz bin of the $\nu_{\rm max}$. In that way, the different contributions of the departure of temperature ($\delta\bar{T}_{\rm eff}(i)$) produced by the gravity-darkening are cancelled (see Section 1). This is only possible if there are a significant amount of stars with a representative amount of different orientations. Then, we only take into account those bins with a population higher than the 1% of the total amount of stars (see Fig. 4). Once with those values, we made the fit finding a linear relation

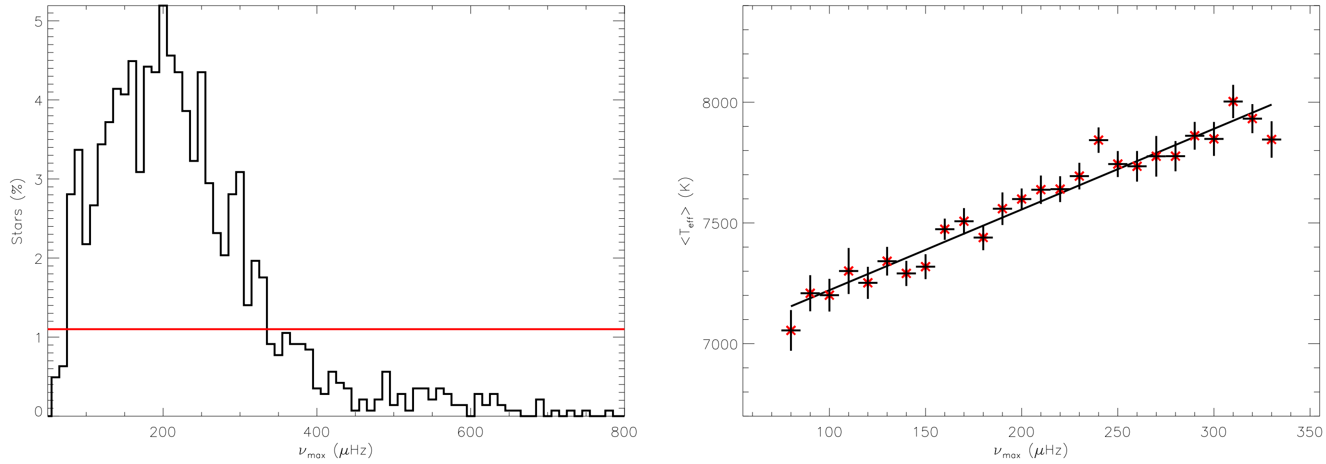

Fig. 4. *Left panel*: Population of stars for each 10 μHz bin of ν_{max}. Red solid line indicates the threshold we used to calculate the MFIT (see text). *Right panel*: Scaling relation found using MFIT.

with a Pearson coefficient of 0.972. The difference between the parameters obtained from the previous technique can be explained with the shorter range we are forced to take.
The third method (KFIT) requires to know the structural parameters of the δ Scuti stars. We selected 8 CoRoT δ Scuti stars from Sismo-channel whose temperature (T_{eff}), rotation rate (Ω/Ω_C) and inclination (i) has been obtained in other studies (see Table 2 in BF18). Using Eq. 4, we can calculate their departure of temperature $\delta\bar{T}_{eff}(i)$ and, finally, its mean effective temperature $\bar{T}_{eff}$. Then, we make the $\bar{T}_{eff} - \nu_{max}$ linear fit. We also find a similar relation than in BF18 but with higher correlation. We noted that the relative differences of mean temperature between all these methods are lower than 5% (see Section 4 for further discussion).

3.2. Mean effective gravity

To study the effect of the evolutionary stage in the frequency distribution, Bowman & Kurtz (2018) analysed the power spectra of a large sample of δ Scuti stars, including hybrids. They separated their sample taking into account the measured effective gravity, g_{eff}, considering three different groups: ZAMS ($log g_{eff} \gtrsim 4.$), MAMS ($3.5 \lesssim log g_{eff} \lesssim 4.0$), and TAMS ($log g_{eff} \lesssim 3.5$), for zero-, mid-, and terminal-age main sequence stars, respectively. They conclude that each evolutionary stage should be treated separately.
Here, we do the same excercise but taking into account the gravity-darkening effect. To calculate the mean effective gravity ($\bar{g}_{eff}$), intrinsic to the star, we use von Zeipel's law (von Zeipel 1924)

$$log\bar{g}_{eff} \approx log g_{eff}(i) - \frac{4}{\beta} log\left(\frac{T_{eff}(i)}{\bar{T}_{eff}}\right), \quad (9)$$

where $\beta \sim 1$ for stars with fully radiative envelope (Claret 1998); and we obtain $\bar{T}_{eff}$ with LFIT scaling relation. Since we can recover $\bar{g}_{eff}$ for 1390 of our δ Scuti stars sample (see Fig. 5), it is possible to observe if the evolutionary stage affects the $\bar{T}_{eff} - \nu_{max}$ relation. In order to study the dependence of the parameters of the scaling relation with $\bar{g}_{eff}$, we divided our sample in several groups of $\Delta \log \bar{g}_{eff} \sim 0.25$ bins.
First of all, we observe that there is a top limit for ν_{max} related to the mean surface gravity (ν_d). To not to take into account spurious candidates, we define this parameter as the top frequency

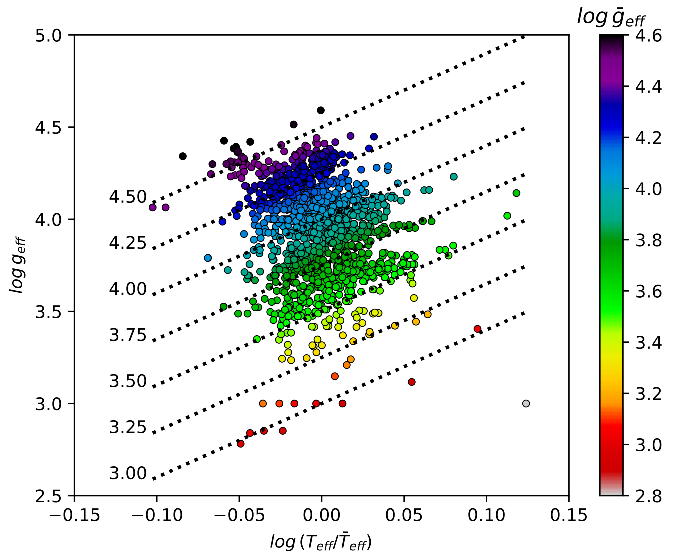

Fig. 5. Measured surface gravity versus the ratio between measured and mean effective temperature. Different colors for each star indicate their mean surface gravity $\bar{g}_{eff}$. Black dotted lines represent the position of the stars with same $\bar{g}_{eff}$ in the diagram but with different departure of temperature.

that contains the 99% of δ Scuti stars of its group (see left panels in Fig. 6). We find its dependence with the mean surface gravity with a linear fit,

$$\nu_d \sim (224 \pm 26)10^{-4}\bar{g}_{eff} + (240 \pm 30) \quad (10)$$

where the frequency is in μHz and the mean surface gravity in c.g.s..
Secondly, we made a $\bar{T}_{eff} - \nu_{max}$ linear fit for each mean surface gravity group (see Fig. 6). We have not taken into account those groups with low population and neither those stars with $\nu_{max} > \nu_d$. In that way, we only take into account those frequency bins with enough stars to cancel the contribution of the gravity-darkening effect (see Section 1). Once with the scaling relation for each $\bar{g}_{eff}$ group (see Table 2), we observed that they change with the mean surface gravity. Then, we calculated the depen-

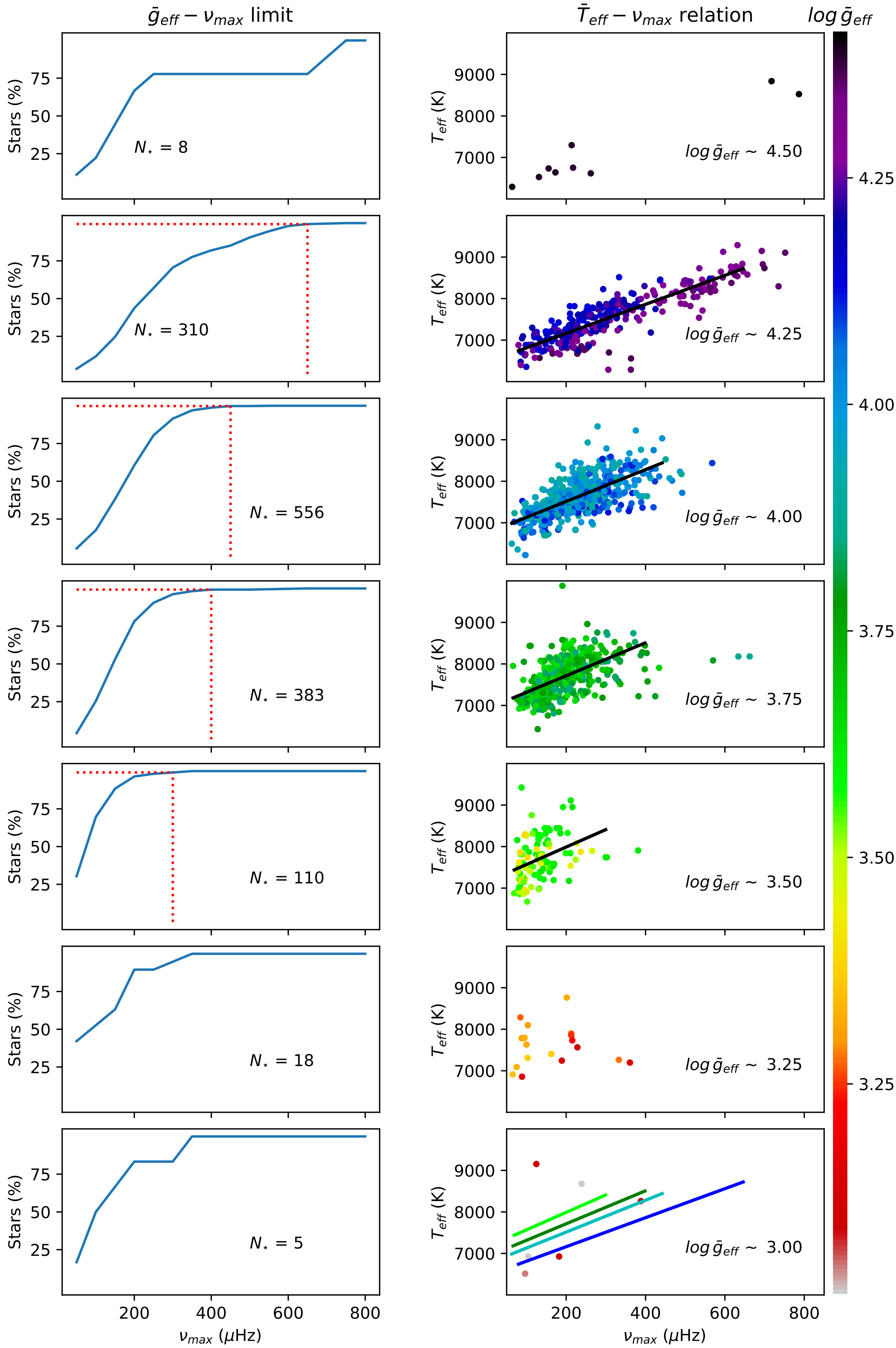

Fig. 6. *From bottom to top, left panels*: Cumulative histogram of the population of stars per $\nu_{\rm max}$ and higher $\bar{g}_{\rm eff}$. Red dotted lines point to the 99% of population limit (see text). We indicate the number of stars per group ($N_\star$). *From bottom to top, right panels*: Relation between $\nu_{\rm max}$ and $\bar{T}_{\rm eff}$ for δ Scuti stars of the same group (solid line, see text). The color of each star indicates its $\bar{g}_{\rm eff}$. *Bottom right panel*: Each coloured line represents the scaling relation for each group.

Table 2. Parameters of the $\bar{T}_{\rm eff} - \nu_{\rm max}$ relation for each $\bar{g}_{\rm eff}$ group

$\log \bar{g}_{\rm eff}$ ± 0.125	Slope (K/μHz)	Y-intercept (K)	σ (%)	r	P_u (%)	$N^{\dagger}_{in}$ (%)	$N^{\dagger}_{out}$ (%)
3.50	4.2 ± 1.1	7150 ± 150	6.43	0.354	15×10^{-7}	99.1	0.9
3.75	4.0 ± 0.3	6920 ± 60	4.96	0.556	19×10^{-35}	99.7	0.3
4.00	3.8 ± 0.2	6750 ± 40	4.25	0.680	11×10^{-79}	99.8	0.2
4.25	3.5 ± 0.1	6460 ± 40	3.36	0.858	4×10^{-93}	100.0	0.0

Notes. $^{(\dagger)}$ Number of stars in and out of the expected departure of temperature limits taking into account $\Omega \sim \Omega_C$ (see text).

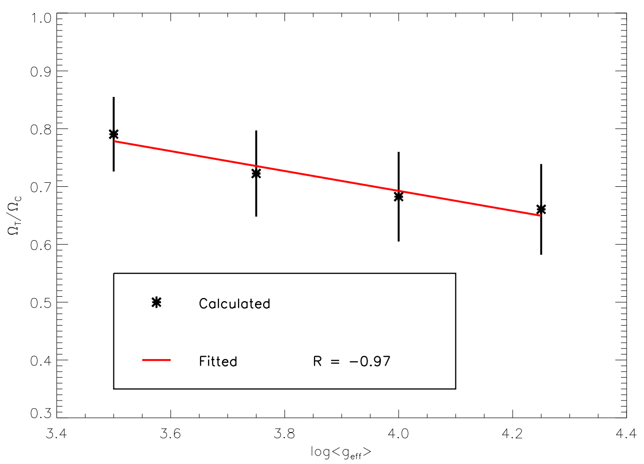

Fig. 7. Typical rotation rate per mean surface gravity for δ Scuti stars. Black asterisks are the calculated values for each group (see text). Red line points to the linear fit.

dence of the slope and the y-intercept with this parameter,

$$\bar{T}_{\rm eff}(\bar{g}_{\rm eff}) \approx (a_1\bar{g}_{\rm eff} + a_2)\,\nu_{\rm max} + (a_3\bar{g}_{\rm eff} + a_4)\ . \tag{11}$$

Once we obtained all parameters (a_i), we use this improved $\bar{T}_{\rm eff}(\bar{g}_{\rm eff}) - \nu_{\rm max}$ relation in Eq. 9 to recalculate the mean surface gravity, improving the selection of the respective group for each star. We repeat all this process, iterating until the variation of the parameters is negligible ($\delta a_i/a_i < 10^{-4}$%). After a few iterations, the parameters of the improved $\bar{T}_{\rm eff}(\bar{g}_{\rm eff}) - \nu_{\rm max}$ scaling relation are

$$\begin{aligned} a_1 &\approx -(46 \pm 5)10^{-6}\,\frac{\rm K\,s^2}{\rm cm\,\mu Hz}\,,\\ a_2 &\approx 4.30 \pm 0.06\,\frac{\rm K}{\rm \mu Hz}\,,\\ a_3 &\approx (44 \pm 6)10^{-3}\,\frac{\rm K\,s^2}{\rm cm}\,,\\ a_4 &\approx 7220 \pm 70\,{\rm K}\,. \end{aligned} \tag{12}$$

Finally, we find a scaling relation between the frequency at maximum power and two intrinsic parameters of δ Scuti star structure.

4. Discussion

We observed that the lowest the surface gravity, the lowest frequency is excited with the same temperature. Then, older stars should have lower frequency ranges as it is predicted by Christensen-Dalsgaard (2000). The highest frequency limit, ~800 μHz, was already pointed by Bowman & Kurtz (2018) although they only take into account the maximum amplitude peak, ν_0, instead of $\nu_{\rm max}$. BF18 proved that there are not significant differences between the use of both parameters to calculate the scaling relation but ν_0 produce a slightly higher dispersion and lower correlation due to the asymmetry of the envelope (see Section 4.2 for further discussion). Then, the discrepancies between both studies can not be produced by the combination frequencies but to take into account hybrid stars. However, to choose a proper parameter to calculate the mean effective temperature is of importance to constrain rotation and inclination for each star (see Section 4.1).

Another phenomenon we observe is a higher dispersion of temperatures for lower $\bar{g}_{\rm eff}$ groups (σ, see Table 1 and Fig. 6). The gravity-darkening effect depends on the ratio between centrifugal and gravity forces, ϵ^2 (see Eq. 4). Rewritting Equation 5 as

$$\epsilon^2 = \frac{\Omega^2 R}{\bar{g}_{\rm eff}} \propto \frac{\Omega^2}{\bar{\rho}}\,, \tag{13}$$

we noted that a higher rotation is required for more dense stars to have the same ϵ^2, i.e., the same departure of temperature. Combining the gravity-darkening effect and the stellar evolution theory, we may explain the behaviour of temperature dispersion since radius increase with age (Christensen-Dalsgaard 2000). Assuming that the observed dispersion (σ) is produced by the gravity-darkening effect, we can define the typical rotation rate (Ω_T) as the minimum rotation needed to observe a departure of temperature equal to σ. We can calculate the minimum rotation rate of a particular departure of temperature assuming a pole-on or equator-on star since intermediate values of inclination require higher values of rotation (see Section 1 and BF18). We use a numerical technique to calculate this parameter (see Section 4.1 for further details). Our results suggest that Ω_T/Ω_C decrease with the mean surface gravity (see Fig. 7) with the form

$$\frac{\Omega_T}{\Omega_C} \approx -(0.17 \pm 0.03)\log \bar{g}_{\rm eff} + (1.38 \pm 0.11)\,, \tag{14}$$

and, therefore, increase with age. This effect does not mean that rotation should increase with age (contrary to gyrochronology predictions; e.g., Soderblom 2010), but it might decrease less than density. In any case, all the values of typical rotation are in agreement with the great fraction of fast rotators for A-type stars found by Royer et al. (2007): $\Omega \gtrsim 0.5\Omega_C$.

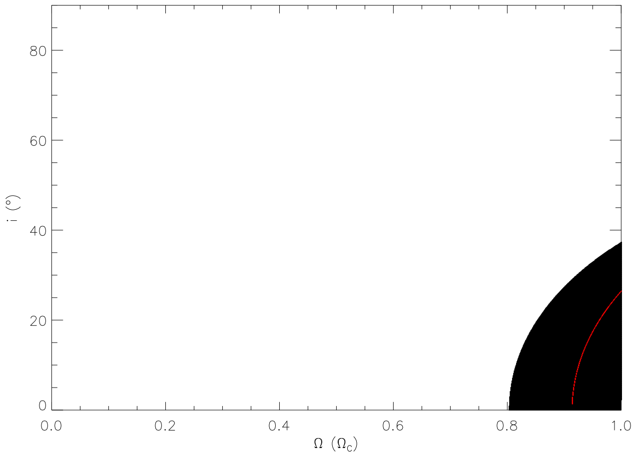

Fig. 8. i–Ω map of the *Kepler* δ Scuti star KIC 11823661. Red points are the models with the exact value of observed departure of temperature. Black points represent those models that take into account the error bars.

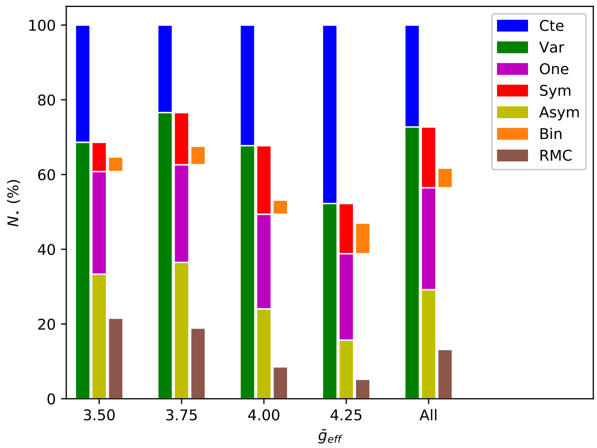

Fig. 9. Proportion of pure δ Scuti stars with constant (Cte) or variable (Var) modes for all the sample and for different evolutionary stage. This last kind can be differentiated with the shape of the multiplet: one sidelobe (One), symmetric (Sym) or asymmetric (Asym) sidelobes. (Bin) indicates the proportion of binary stars detected with this method (see text). RMC indicates the proportion of this kind of stars that show multiplets affected by resonant mode coupling (see text).

4.1. $i-\Omega$ maps

BF18 calculated the minimum rotation rate ($\Omega_{\rm min}$) for ~700 pure δ Scuti stars. This parameter can be obtained using Eq. 4 and assuming the star is pole-on or equator-on. Furthermore, the limits of the inclination from the line of sight (i) can also been obtained assuming $\Omega \sim \Omega_C$. But, the observed departure of temperature should be higher than the relative error of the measurement

$$\delta\bar{T}_{\rm eff,obs} > ET_{\rm eff}/\bar{T}_{\rm eff}\,, \qquad (15)$$

to avoid the $i-\Omega$ degeneracy zone (see Fig 5 and 6 in BF18). This zone do not allow us to use this technique to differentiate between a moderate or slow rotator with any inclination from a extreme rotator with an inclination close to the mid-latitude ($i \sim 55°$). In that case a deeper study is needed (e.g., Poretti et al. 2009; García Hernández et al. 2013; Escorza et al. 2016; Barceló Forteza et al. 2017).

We used a different technique to obtain a map with all possible combinations of $i-\Omega$. This method consits to simulate around one million of stars with different $i-\Omega$ values and only select those which fulfil the observed departure of temperarure $\delta\bar{T}_{\rm eff,obs}$ (see Fig. 8).

To calculate the correct $\delta\bar{T}_{\rm eff,obs}$, we take into account the improved scaling relation (Eq. 11). But it is not always possible since we may not know the measured $g_{\rm eff}$. In that case we use the LFIT scaling relation. The limits of rotation and inclination for the stars of our sample (see Table A.1), including $i-\Omega$ maps, are only available in electronic form.

In this way, we find only five δ Scuti stars are out of the expected regime of temperature for fast rotators: $\delta T_{\rm eff,obs} \lesssim -21.5\%$ or $\delta T_{\rm eff,obs} \gtrsim 14.5\%$. The other 4 outsiders have an unknown value of surface gravity. These stars may be (pre-)Extremely Low Mass stars since they have similar frequency ranges and similar or higher surface gravity (Sánchez Arias et al. 2018).

4.2. Mode variations with time

There are several reasons to use $\nu_{\rm max}$ instead of ν_0 apart from its lower dispersion. First of all, the visibility of the highest amplitude mode depends of the point of view of the observer (see Lignières & Georgeot 2009). Secondly, the highest amplitude mode is not fixed, i.e., the amplitudes can change with time and other modes can relieve the highest amplitude mode (i.e., Handler et al. 1998; Breger 2000b; Barceló Forteza et al. 2015). This is not the case for $\nu_{\rm max}$ that remains approximately constant during the cyclic changes (see Fig 10). To study the variability of ν_0 and $\nu_{\rm max}$ with time for stars with detected cyclic variations, we used δSBF pipeline for each 20-d segments and we compared the results with these of the entire light curve. To find a sample of stars with cyclic variations, we studied the power spectrum of the entire light curve for all pure δ Scuti stars of our sample. There, the variations in the parameters of a mode are observed as split peaks of this mode (e.g., Moskalik 1985; Shibahashi & Kurtz 2012), i.e., a multiplet. The frequency shift between peaks, the ratio of amplitudes, and the symmetry of the multiplet may indicate the nature of the variation. On one hand, a symmetric multiplet could indicate a superNyquist frequency mode (Murphy et al. 2013) or a binarity nature of the system (e.g., Shibahashi & Kurtz 2012; Murphy et al. 2014). On the other hand an asymmetric multiplet can indicate a cyclic variation such as resonant mode coupling (RMC; Moskalik 1985; Barceló Forteza et al. 2015) or, in the case of only one sidelobe, may suggest a definitive change in the stellar structure (Bowman et al. 2016). Fig. 10 show the variation of ν_0 and $\nu_{\rm max}$ for 5 pure δ Scuti stars with detected variations in some of their peaks in agreement with RMC. The sharp changes of ν_0 with time can be compared with $\nu_{\rm max}$ 20-d measurements. In fact, the ν_0 mean of the 20-d light curves is not in agreement with the value obtained with the entire light curve in all tested cases. This is not the case for $\nu_{\rm max}$ since both values are equal within errors. Resonances seem not to modify $\nu_{\rm max}$ at least in the long term.

In this study, we also find that only 27% of pure δ Scuti stars have constant amplitude peaks (see Fig.9). We recover the same proportion of stars with constant modes obtained by Bowman et al. (2016) if we take into account hybrid stars (38%). We observed that the other 73% of the pure δ Scuti stars have modes with detected amplitude and/or phase variations. Looking to these phenomena for each $\bar{g}_{\rm eff}$ group, we observe

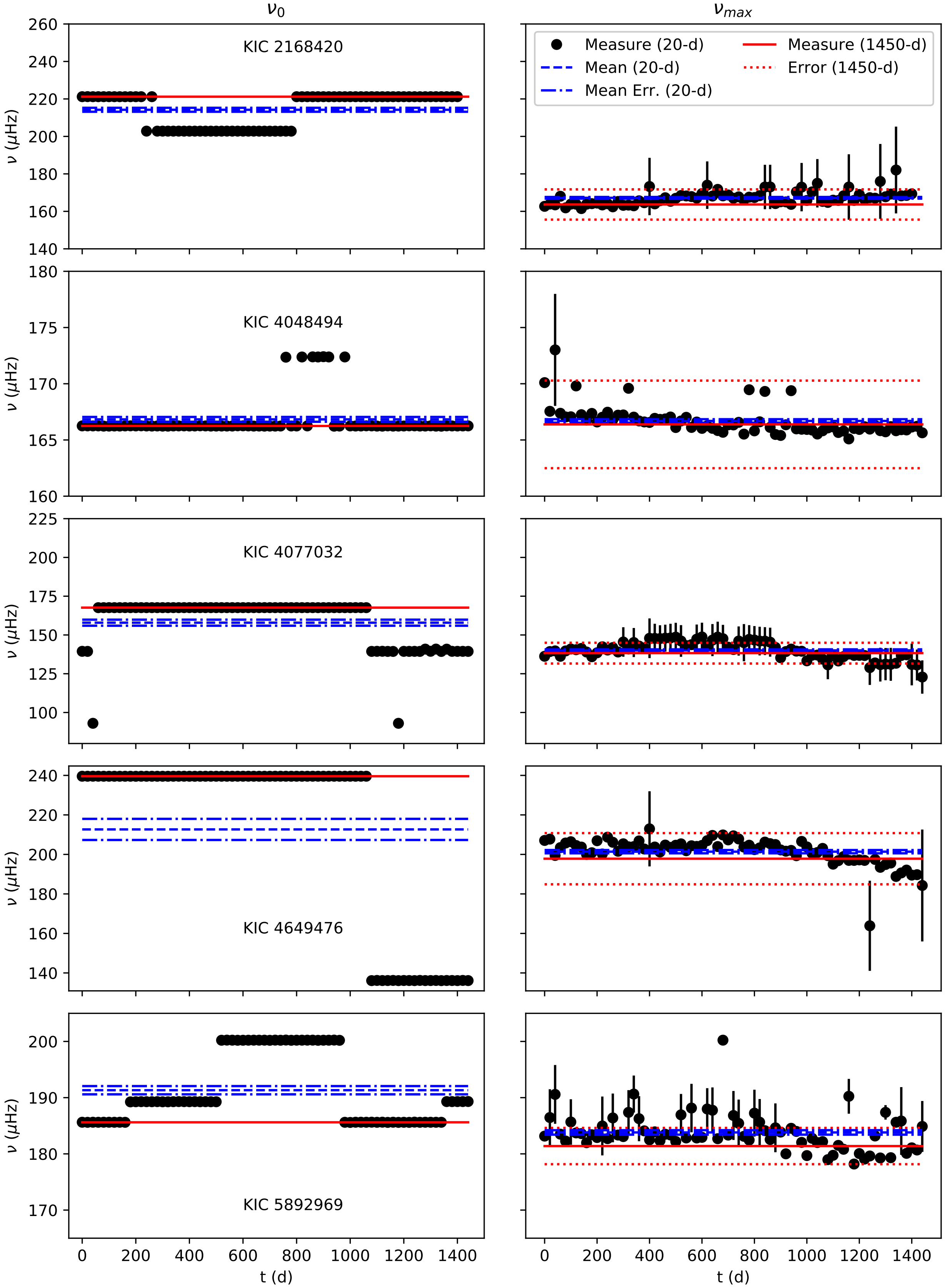

Fig. 10. Frequency of the highest amplitude peak (ν_0, left panels) and frequency at maximum power (ν_{max}, right panels) with time for five pure δ Scuti stars with detected RMC (one per row; see text). Black circles represent the measurements of each parameters for 20-day segments of the entire light curve. Blue dashed line is the mean value of all 20-d measurements and blue dashed-dotted lines are their error. Red line is the measurement of each parameter for a 1450-day light curve and red dotted lines are their error. The error bars for 20-d measurements of ν_0 are smaller than the symbol. For clarity reasons, we only plotted the error bars for 20-d measurements of ν_{max} for these outside of the 1450-d measure error.

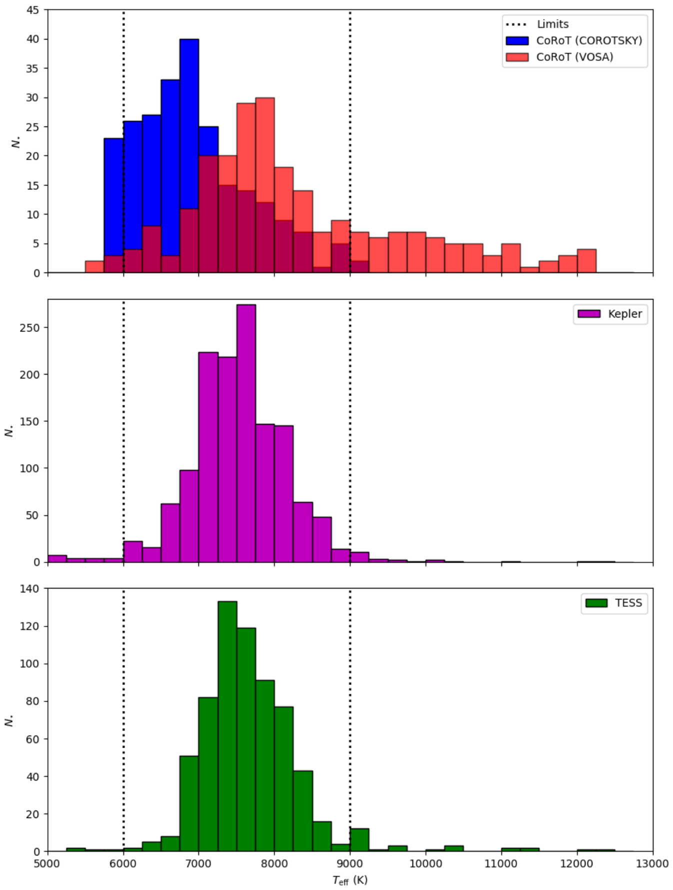

Fig. 11. Top panel: Histogram of temperatures for 239 δ Scuti star candidates observed by *CoRoT*. Blue bars point to values from COROTSKY database (Charpinet et al. 2006) and red bars point to these obtained with VOSA (see text). Dotted lines represent the temperature limits for δ Scuti stars (Uytterhoeven et al. 2011). Middle and bottom panels: Same as top panel for stars of our main sample observed by *Kepler* and *TESS*, respectively.

significant differences. The lowest the surface gravity, the high amount of δ Scuti stars with detected variable modes (from 52% to 76%), especially for those with asymmetric multiplets (from 16% to 35%), including these candidates to have RMC (from 5% to 20%). Moreover, these candidates with extrinsic causes of variation (superNyquist frequencies or binarity) are approximately constant with surface gravity (∼16%). Finally, the proportion of stars observed with multiplets of only one detected sidelobe is approximately constant too (∼27%). We also added this analysis star by star in Table A.1.

Our results suggest that the evolutionary stage seems to favour resonances towards older ages. This is in agreement with the increase of the g-mode frequencies with age (Christensen-Dalsgaard 2000) and its interaction with p-modes. In addition, the transition stages may be observed as permanent changes in the power spectra of the stars due to their restructuring.

5. Advantages of $\bar{T}_{\rm eff}$

Once with the parameters of the scaling relation, we can use Eq. 11 to obtain the mean effective temperature of other pure δ Scuti stars. We analysed the power spectra of 239 δ Scuti candidates observed by CoRoT Exo-channel (Debosscher et al. 2009), calculating their $\bar{T}_{\rm eff}$ for 174 of them (see Table A.2 only in the electronic form). The $T_{\rm eff}$ of these stars were estimated by fitting their spectral energy distribution (SED) to a grid of theoretical models (Kurucz, Castelli et al. 1997) using the Virtual Observatory tool (VOSA, Bayo et al. 2008). Extinction was left as a free parameter in the SED fitting process, ranging from zero to the value obtained from the NASA/IPAC Galactic Dust Reddening and Extinction service[1] using (Schlafly & Finkbeiner 2011)

Figure 11 compares the effective temperatures obtained with VOSA (red bars) with those available in the COROTSKY Database (blue bars; Charpinet et al. 2006). We can see how the assumption of no extinction for the majority of the objects in COROTSKY leads to an underestimation of the temperatures. This effect may cause a misclassification since low temperature δ Scuti stars will not be considered and too high temperature pulsators of other kinds will.

Moreover, different models based on different physical properties, may produce results with discrepancies up to the same order of magnitude (Sarro et al. 2013). For example, rotation can modify the observed colors (Collins & Smith 1985) with the consequent impact on temperature. In contrast, $\bar{T}_{\rm eff}$ seem not to depend on these parameters. Therefore, we can conclude that the scaling relation based on $\nu_{\rm max}$ allow us to characterize δ Scuti stars independently of rotation and also extrinsic parameters of the star such as extinction.

6. Conclusions

Once characterized the power spectra of 1442 pure δ Scuti stars observed by *CoRoT*, *Kepler* & *TESS*, we recover the linear relation between the frequency at maximum power and the mean effective temperature found by Barceló Forteza et al. (2018). This is in agreement with the predicted frequency distribution of κ-mechanism since we detected higher frequency modes for higher temperature δ Scuti stars. We also observed that old stars with low surface gravity present lower frequency ranges, just as opposite than young δ Scuti stars. This is in agreement with predictions too. Therefore, the evolutionary stage also affects the empirical scaling relation and it must be taken into account to find the intrinsic parameters of these kind of stars ($\bar{T}_{\rm eff}, \bar{g}_{\rm eff}$). We suggest that both evolutionary stage and gravity-darkening effect may play important roles to explain the observed dispersion and its variation. Thanks to these properties it is possible to delimit rotation and inclination from the line of sight, especially for fast rotators. Finally, we suggest $\nu_{\rm max}$ as a seismic index since seems to be a proper indicative of the mean temperature of the star (see Eq. 11) and it is not as affected as ν_0 with rotation, inclination, and/or resonances. Its variation may indicate the restructuring of the stars and their power spectra between different transition stages.

Acknowledgements. Authors wish to thank the *CoRoT*, *Kepler*, and *TESS* Teams whose efforts made these results possible. The *CoRoT* space mission has been developed and was operated by *CNES*, with contributions from Austria, Belgium, Brazil, ESA (RSSD and Science Program), Germany and Spain. Funding for *Kepler*'s Discovery mission is provided by NASA's Science Mission Directorate. Funding for the TESS mission is provided by the NASA Explorer Program. Authors acknowledge the effort made by TASOC WG4 that helped us in our target selection. This publication makes use of VOSA, developed under the Spanish Virtual Observatory project supported by the Spanish MINECO through grant AyA2017-84089. VOSA has been partially updated by using funding from the European Union's Horizon 2020 Research and Innovation Programme, under Grant Agreement No 776403 (EXOPLANETS-A).

[1] https://irsa.ipac.caltech.edu/applications/DUST/

SBF and DB has received financial support from the Spanish State Research Agency (AEI) Projects No.ESP2017-87676-C5-1-R and No. MDM-2017-0737 Unidad de Excelencia "María de Maeztu"- Centro de Astrobiología (INTA-CSIC). AM acknowledges funding from the European Union's Horizon 2020 research and innovation program under the Marie Sklodowska-Curie grant agreement No 749962 (project THOT). SMR acknowledges financial support from the State Agency for Research of the Spanish MCIU through the "Center of Excellence Severo Ochoa" award to the Instituto de Astrofísica de Andalucía (SEV-2017-0709). JCS and AGH acknowledges funding support from Spanish public funds (including FEDER fonds) for research under project ESP2017-87676-C5-2-R and ESP2017-87676-C5-5-R. JCS also acknowledges support from project RYC-2012-09913 under the 'Ramón y Cajal' program of the Spanish Ministry of Science and Education.

References

Aerts, C., Christensen-Dalsgaard, J., & Kurtz, D. W. 2010, Asteroseismology
Antoci, V., Cunha, M., Houdek, G., et al. 2014, ApJ, 796, 118
Baglin, A., Auvergne, M., Barge, P., et al. 2006, in ESA Special Publication, Vol. 1306, ESA Special Publication, ed. M. Fridlund, A. Baglin, J. Lochard, & L. Conroy, 33
Balona, L. A. & Dziembowski, W. A. 2011, MNRAS, 417, 591
Barceló Forteza, S., Michel, E., Roca Cortés, T., & García, R. A. 2015, A&A, 579, A133
Barceló Forteza, S., Roca Cortés, T., & García, R. A. 2018, A&A, 614, A46
Barceló Forteza, S., Roca Cortés, T., García Hernández, A., & García, R. A. 2017, A&A, 601, A57
Bayo, A., Rodrigo, C., Barrado Y Navascués, D., et al. 2008, A&A, 492, 277
Borucki, W. J., Koch, D., Basri, G., et al. 2010, Science, 327, 977
Bowman, D. M. & Kurtz, D. W. 2018, MNRAS, 476, 3169
Bowman, D. M., Kurtz, D. W., Breger, M., Murphy, S. J., & Holdsworth, D. L. 2016, MNRAS, 460, 1970
Breger, M. 2000a, in Astronomical Society of the Pacific Conference Series, Vol. 210, Delta Scuti and Related Stars, ed. M. Breger & M. Montgomery, 3
Breger, M. 2000b, MNRAS, 313, 129
Brown, T. M., Latham, D. W., Everett, M. E., & Esquerdo, G. A. 2011, AJ, 142, 112
Castelli, F., Gratton, R. G., & Kurucz, R. L. 1997, A&A, 318, 841
Charpinet, S., Cuvilo, J., Platzer, J., et al. 2006, in ESA Special Publication, Vol. 1306, The CoRoT Mission Pre-Launch Status - Stellar Seismology and Planet Finding, ed. M. Fridlund, A. Baglin, J. Lochard, & L. Conroy, 353
Chevalier, C. 1971, A&A, 14, 24
Christensen-Dalsgaard, J. 2000, in Astronomical Society of the Pacific Conference Series, Vol. 210, Delta Scuti and Related Stars, ed. M. Breger & M. Montgomery, 187
Claret, A. 1998, A&AS, 131, 395
Collins, G. W., I. & Smith, R. C. 1985, MNRAS, 213, 519
de Franciscis, S., Pascual-Granado, J., Suárez, J. C., et al. 2019, MNRAS, 487, 4457
Debosscher, J., Sarro, L. M., López, M., et al. 2009, A&A, 506, 519
Dziembowski, W. 1997, in IAU Symposium, Vol. 181, Sounding Solar and Stellar Interiors, ed. J. Provost & F.-X. Schmider, 317
Escorza, A., Zwintz, K., Tkachenko, A., et al. 2016, A&A, 588, A71
García, R. A., Mathur, S., Pires, S., et al. 2014, A&A, 568, A10
García Hernández, A., Martín-Ruiz, S., Monteiro, M. J. P. F. G., et al. 2015, ApJ, 811, L29
García Hernández, A., Moya, A., Michel, E., et al. 2013, A&A, 559, A63
Handler, G., Pamyatnykh, A. A., Zima, W., et al. 1998, MNRAS, 295, 377
Kjeldsen, H. & Bedding, T. R. 1995, A&A, 293, 87
Lignières, F. & Georgeot, B. 2009, A&A, 500, 1173
Michel, E., Dupret, M.-A., Reese, D., et al. 2017, in European Physical Journal Web of Conferences, Vol. 160, European Physical Journal Web of Conferences, 03001
Moskalik, P. 1985, Acta Astron., 35, 229
Moya, A., Suárez, J. C., García Hernández, A., & Mendoza, M. A. 2017, MNRAS, 471, 2491
Murphy, S. J., Bedding, T. R., Shibahashi, H., Kurtz, D. W., & Kjeldsen, H. 2014, MNRAS, 441, 2515
Murphy, S. J., Shibahashi, H., & Kurtz, D. W. 2013, MNRAS, 430, 2986
Pérez Hernández, F., Claret, A., Hernández, M. M., & Michel, E. 1999, A&A, 346, 586
Poretti, E., Michel, E., Garrido, R., et al. 2009, A&A, 506, 85
Royer, F., Zorec, J., & Gómez, A. E. 2007, A&A, 463, 671
Sánchez Arias, J. P., Romero, A. D., Córsico, A. H., et al. 2018, A&A, 616, A80
Sarro, L. M., Debosscher, J., Neiner, C., et al. 2013, A&A, 550, A120
Schlafly, E. F. & Finkbeiner, D. P. 2011, ApJ, 737, 103
Shibahashi, H. & Kurtz, D. W. 2012, MNRAS, 422, 738
Soderblom, D. R. 2010, ARA&A, 48, 581
Stassun, K. G., Oelkers, R. J., Paegert, M., et al. 2019, AJ, 158, 138
Suárez, J. C., García Hernández, A., Moya, A., et al. 2014, A&A, 563, A7
Taylor, J. 1997, Introduction to Error Analysis, the Study of Uncertainties in Physical Measurements, 2nd Edition (University Science Books)
Uytterhoeven, K., Moya, A., Grigahcène, A., et al. 2011, A&A, 534, A125
von Zeipel, H. 1924, MNRAS, 84, 684
Xiong, D. R., Deng, L., Zhang, C., & Wang, K. 2016, MNRAS, 457, 3163